Poisson-Nernst-Planck Equations for Simulating Biomolecular Diffusion-Reaction Processes I: Finite Element Solutions

Benzhuo Lu[a], **Michael J. Holst**[b,c], **J. Andrew McCammon**[d,c,e], and **Y. C. Zhou**[f,1]

[a] State Key Laboratory of Scientific and Engineering Computing, Institute of Computational Mathematics and Scientific/Engineering Computing, Academy of Mathematics and Systems Science, Chinese Academy of Sciences, Beijing 100190, China

[b] Department of Mathematics, University of California San Diego, La Jolla, CA 92093, USA

[c] Center for Theoretical Biological Physics, University of California San Diego, La Jolla, CA 92093, USA

[d] Department of Chemistry and Biochemistry, University of California San Diego, La Jolla, CA 92093, USA

[e] Department of Pharmacology, University of California San Diego, La Jolla, CA 92093, USA

[f] Department of Mathematics, Colorado State University, Fort Collins, CO 80523, USA

Abstract

In this paper we developed accurate finite element methods for solving 3-D Poisson-Nernst-Planck (PNP) equations with singular permanent charges for electrodiffusion in solvated biomolecular systems. The electrostatic Poisson equation was defined in the biomolecules and in the solvent, while the Nernst-Planck equation was defined only in the solvent. We applied a stable regularization scheme to remove the singular component of the electrostatic potential induced by the permanent charges inside biomolecules, and formulated regular, well-posed PNP equations. An inexact-Newton method was used to solve the coupled nonlinear elliptic equations for the steady problems; while an Adams-Bashforth-Crank-Nicolson method was devised for time integration for the unsteady electrodiffusion. We numerically investigated the conditioning of the stiffness matrices for the finite element approximations of the two formulations of the Nernst-Planck equation, and theoretically proved that the transformed formulation is always associated with an ill-conditioned stiffness matrix. We also studied the electroneutrality of the solution and its relation with the boundary conditions on the molecular surface, and concluded that a large net charge concentration is always present near the molecular surface due to the presence of multiple species of charged particles in the solution. The numerical methods are shown to be accurate and stable by various test problems, and are applicable to real large-scale biophysical electrodiffusion problems.

Keywords

Electrodiffusion; Poisson-Nernst-Planck equations; Finite element; Singular charges; Molecular surface; Boundary condition; Conditioning

---

[1]Corresonding author. yzhou@math.colostate.edu.

1. Introduction

Electrodiffusion is a rate-limiting step in numerous biological processes, such as ligand-enzyme binding, protein-protein diffusive encounter. An example is neurotransmission within synapses between adjacent nerve cells [6]. The kinetic properties of these processes are mostly governed by the multi-scale electrodiffusion of charged molecules in aqueous solution with various ionic concentrations, molecular charges and complicated solvent-solute interface geometries. The numerical techniques for quantitatively determining the kinetic parameters generally fall into categories of particle-based and continuum methods. The former includes Monte Carlo (MC) [23], Brownian dynamics (MD) [16] and Langevin dynamics (LD) [40]. These methods trace the trajectories of individual particles in appropriate energy landscape and thus have a nature of discrete and stochastic. Consequently they might suffer a divergence when applied to systems with a large amount of particles. The continuum models, in contrast, focus on the average density distribution of species of charged particles and their description through unified partial differential equations. It is therefore computationally more efficient to apply the continuum models for simulating multiple species and large systems. Furthermore, continuum electrodiffusion models can be readily modified to incorporate more types of physical interactions, such as varying molecular surface or flow convection, by coupling with elasticity equation or the Navier-Stokes equations. These appealing features have made the continuum electrodiffusion models very useful not only for the quantitative analysis of the biologcal ion channels [18,20] and cellular electrophysiology [38,39], but also for investigating ion separation membranes in non-biological applications [45] and the transport of electrons and holes in semiconductors [28].

In this work we adopt the Poisson-Nernst-Planck equations to describe the electrodiffusion of mobile ions and charged ligands, all modeled as diffusive particles with vanishing size, in solvated biomolecular systems. Here the electrostatic potential is induced by the mobile ions, charged ligands, and the fixed charges carried by biomolecules. Figure (1) illustrates a solvated biomolecular system in an open domain $\Omega \in \mathbb{R}^3$. The open domain $\Omega_m \subset \Omega$ represents the biomolecule(s), and the remaining space $\Omega_s = \Omega \backslash \Omega_m$ is filled with aqueous solvent. Domains Ω_m and Ω_s are separated by a molecular surface Γ, which can be defined as the solvent accessible surface, Gaussian surface [52], or some other appropriately defined solvent-molecular interface that is Lipschitz continuous. The diffusive particles are distributed in Ω_s. Charged ligands might react with the biomolecules on a part of the molecular surface Γ_a, for which a suitable boundary condition for the diffusion equations of the particles is needed. On the non-reactive molecular surface $\Gamma \backslash \Gamma_a$ appropriate boundary condition is needed to model the vanishing macroscopic flux. In a typical solvated biomolecular system there are multiple species of ions and ligands; each species may have its own boundary condition on molecular surface. We assume that the exterior boundary $\partial\Omega$ is connected to a particle reservoir maintained at constant concentrations, and hence a Dirichlet boundary condition for particle concentration can be applied. Compared to the pure diffusion [51], or the Nernst-Planck equation (also called Smoluchowski equation) [50] which characterizes diffusional drift by a given fixed potential, the Poisson-Nernst-Planck model is able to generate a self-consistent electrostatic potential and the non-equilibrium densities [55]. It is worth noting that the PNP equations for describing the electrodiffusion around the biomolecules modeled at atomistic level have two unique features, i.e., the presence of the singular permanent charges inside biomolecules and that the biomolecules with highly irregular surfaces are not penetrable to diffusive particles. These features have to be delicately treated to establish sound mathematical analysis and highly accurate, efficient numerical treatments for the 3-D PNP equations. Thanks to the rapid development of X-ray crystallography, nuclear magnetic resonance (NMR), Cryo-electron microscopy techniques

and some accurate structure refinement algorithms, the determination of macromolecular structures with increasing resolution in the recent decades provides the structural and geometrical basis for these studies.

Mathematical analyses of the Poisson-Nernst-Planck equations have been developed long after the introduction of the equation by Nernst and Planck [41,42]. The existence and stability for the solutions of the steady PNP equations are established by Jerome [29] in studying the steady Van Roost-broeck model for electron flows in semiconductors, via a delicate construction of a Schauder fixed point mapping. Although this mapping is not shown to be contractive, an alternative pseudo-monotone mapping is constructed which guarantees the convergence of the Galerkin approximations of the equations. It it noted that the permanent charges in this study are located in the same domain as the diffusion process, and are assumed to be in L^∞ which ensures the $H^1 \cap L^\infty$ regularity of the electrostatic potential and the charge densities. Existence and long time behavior of the unsteady PNP equations were studied in [7]. The analysis and computation of the PNP equations can be further simplified by reducing the 3-D system to 1-D models. Singular perturbation methods and asymptotic analysis can then be applied to study the solution properties of these simplified 1-D equations. For example, 1-D steady PNP equations for modeling physiological channels are investigated in [5,33] in the absence of permanent charges by using various singular perturbation theories. The effects of the permanent charges are considered in [17,1], where the permanent charge density is vanishing in the reservoirs at the two ends of the channel and is constant at the center of the channel. The piecewise constant form of the permanent charges implies that the electrostatic potential and ionic densities are still differentiable. The reduction of the dimensionality greatly simplifies the mathematical analysis of the electrodiffusion systems, and the results provide useful guide lines for the analysis of the corresponding fully 3-D systems at some limit cases. As a trade-off they are generally unable to reproduce the diffusion and reaction processes that critically depend on the geometry of the system and complicated boundary conditions.

In contrast to the limited amount of work on the mathematical analysis of the PNP equations for biophysical applications, numerical computations with the PNP and the PNP-like systems have been widely conducted by computational physicists and biophysicists. Finite difference methods are particularly popular due to the simplicity in their implementation, and have been applied to a large extent to 1-D or 3-D ion conduction characteristics of biological ion channels or other transmembrane pores [14,18,31,10,8]. The lattice nature of the finite difference method makes it difficult to model the highly irregular surface of the ion channel or the active sites of the enzymes. This difficulty can be readily overcome by using finite element methods, which have been well developed for simulating semiconductor devices [30,19] and were recently introduced to simulate the electrodiffusion with realistic molecular structures [50,49]. In many of the PNP solvers developed thus far such as [31,10,8] the electrostatic part is solved by using well-established finite difference or finite element Poisson-Boltzmann solvers [37,9,3]. These PB solvers use polynomial interpolations to approximate the singular charges. When the electrostatic solvation energies are concerned, the errors caused by these interpolations are generally acceptable [22,21]. However, the singular nature of the permanent charges suggests that the electrostatic potential and its gradient near the molecular surface is large indeed. Proper treatments of these singular charges must be devised to solve the electrostatic potential with sufficient accuracy to supply an electric field of high fidelity to the Nernst-Planck equation. It is proposed [21,13] that the singular component of the electrostatic potential can be removed through a proper decomposition of the Poisson-Boltzmann equation, and a regular component can be solved numerically from an elliptic interface problem. The numerical properties of these decomposition schemes are analyzed [11,27]. In particular, it is shown that an elegant decomposition of potential into a singular component, a harmonic component

and the regular component can significantly improve the accuracy of the total potential, especially the potential in the solvent region [27].

The objective of the this paper is threefold: to introduce the stable regularization to the numerical solutions of the Poisson-Nernst-Planck equations with singular permanent charges; to develop finite element methods for solving the regular PNP equations with realistic biomolecular structures; and to apply the numerical methods to investigate the properties of the equations, such as the self-adjoint transformation, conditioning, the electroneutrality assumption and its dependence on the strength of the electrostatic potential and the boundary conditions. We will show that the electrostatic potential that couples the Nernst-Planck equation is indeed the regular component. Therefore the framework established in [29] for general L_2 permanent charges could be utilized to show the well-posedness of the regularized PNP system. An inexact-Newton method will be used to solve the nonlinear differential equations. Since the Poisson-Nernst-Planck equations can be derived from the first variations of a free energy functional, the Newton-like methods can produce a convergent solution that corresponds to the minimization of the free energy.

The rest of the paper is organized as follows. The Poisson-Nernst-Planck equations are introduced in Section 2 following a brief history of the equations. Two regularization schemes are then described and their numerical properties are discussed. The properties of the regular nonlinear equations will be summarized also. Section 3 is devoted to the Galerkin approximation of the regularized PNP equations. The inexact-Newton method is applied to bilinear weak form of the equations, for both the steady and the time-dependent problems. Numerical examples are given in Section 4. The accuracy of the method and the usefulness of two formulations of the Nernst-Planck equation will be examined. We will vary the boundary conditions of the sample problems to investigate the validity of the electroneutrality. The method will be finally applied to compute the diffusion of charged ligands in the solution around acetylcholinesterase (AChE) enzyme to demonstrate its usefulness for real biological problems. The paper ends with a summary in Section 5.

2. Mathematical Models

The continuum PNP equations can be derived via different routes. They can be obtained from the microscopic model of Langevin trajectories in the limit of large damping and absence of correlations of different ionic trajectories [47,40], or from the variations of the free energy functional that includes the electrostatic free energy and the ideal component of the chemical potential [20]. The former gives the PNP model a sound theoretical basis while the latter provides a flexible framework to include more physical interactions, most prominently the correlations among particles with finite sizes, into the continuum model. In this work, we are concentrated in the development of numerical techniques for the standard nonlinear PNP equations, i.e., we treat all diffusive particles, including mobile ions and charged ligands, as particles with vanishing size. This is a reasonable assumption in case that solution is dilute and the characteristic dimension of space for diffusion is much larger than the particle size.

We obtain the PNP equations by coupling the Nernst-Planck equation

$$\frac{\partial \rho_i}{\partial t} = \nabla \cdot D_i (\nabla \rho_i + \beta q_i \rho_i \nabla \varphi), \quad x \in \Omega_s, \quad 1 \le i \le n, \tag{1}$$

and the electrostatic Poisson equation with internal interface $\Gamma = \bar{\Omega}_s \cap \bar{\Omega} m$:

$$-\nabla \cdot (\varepsilon \nabla \varphi) - \lambda \sum_i q_i \rho_i = \rho^f, \quad x \in \Omega,$$

(2)

$$\varphi_m = \varphi_s, \quad \varepsilon_m \frac{\partial \varphi_m}{\partial n} = \varepsilon_s \frac{\partial \varphi_s}{\partial n} \quad x \in \Gamma,$$

(3)

where $\rho_i(x, t)$ is the concentration of the i-th species particles carrying charge q_i, $D_i(x)$ is the spatial-dependent diffusion coefficient, and φ is the electrostatic potential. The constant $\beta = 1/(k_B T)$ is the inverse Boltzmann energy where k_B is the Boltzmann constant and T is the absolute temperature. We assume that the dielectric permittivity is a piecewise constant with $\varepsilon = \varepsilon_m \varepsilon_0$ in Ω_m and $\varepsilon = \varepsilon_s \varepsilon_0$ in Ω_s, where ε_0 is the dielectric constant of vacuum. This is a standard assumption in most implicit solvent models [2], and is indispensable to the regularization schemes to be introduced later. The internal dielectric interface separating the molecules and solvent regions is defined to be the molecular surface, but other definitions of dielectric interface might apply also. Typical values of ε_m and ε_s are 2 and 80, respectively. The permanent (fixed) charge distribution

$$\rho^f(x) = \sum_j q_j \delta(x - x_j)$$

is an ensemble of singular charges q_j located at x_j inside biomolecules. The characteristic function λ is equal to 1 in Ω_s and 0 in Ω_m, suggesting that mobile ions are present only in the solvent region. If the mobile charge density $\rho_i(x)$ in Eq. (2) is assumed to follow the Boltzmann distribution, the equation converts to the nonlinear Poisson-Boltzmann equation. The readers are referred to [34] for detailed discussions on the derivation and relations of these equations. The time-dependence of the electrostatic potential is seen from the appearance of time-dependent particle concentrations in Eq. (2). The ellipticity of the steady-state equations suggests that the relaxation of electrostatic potential field in response to the variation of particle concentrations is instantaneous, similar to the relaxation of pressure in response to varying velocity field of incompressible flow field. This similarity offers useful guidelines in developing numerical methods for the PNP model, as we shall see in the next section.

Numerical solution of the electrostatic Poisson equation in the PNP model above warrants appropriate approximation of the singular charge $\rho^f(x)$. In many finite difference or finite element solvers of the Poisson-Boltzmann equation, the singular charges are distributed onto the grid points near the singular charges by using spline interpolations. These approximations work well when the electrostatic potentials are used to compute the electrostatic free energy and other energy quantities [9,54]. If the gradient of the electrostatic potential is needed, such as the PNP equations studied here, more rigorous treatments of the singular charges are needed. The first approach is proposed by Gilson *et. al.* [21]; they characterize the singular component of the electrostatic potential through a Poisson equation with singular charges only:

$$-\varepsilon_m \Delta \varphi^s = \rho^f(x), \quad x \in \mathbb{R}^3.$$

(4)

Subtracting this singular component from Eq. (2) we get the equation for the regular component:

$$-\nabla \cdot (\varepsilon \nabla \varphi^r(x,t)) - \lambda \sum_i q_i \rho_i(x,t) = 0, \quad x \in \Omega.$$

(5)

The singular component φ^s should also be subtracted from the interface conditions (3), generating the following interface conditions for Eq. (5):

$$\varphi_s^r - \varphi_m^r = 0, \quad \varepsilon_s \frac{\partial \varphi_s^r}{\partial n} - \varepsilon_m \frac{\partial \varphi_m^r}{\partial n} = (\varepsilon_m - \varepsilon_s) \frac{\partial \varphi^s}{\partial n}, \quad x \in \Gamma.$$

(6)

This approach is applied to solve the Poisson-Boltzmann equation by Zhou *et. al.* [56] to completely remove the self-energy so that the equation need not to be solved twice for computing the electrostatic energy. The removal of the singular potential makes it possible for the first time to analyze the Poisson-Boltzmann equation rigorously in Sobolev spaces [11]. However, it is found that this method suffers a numerical instability that will lead to a substantial error in the numerical solution of the full potential [27]. This is because that the total potential φ is relatively weak while the singular potential φ^s and the regular potential are both strong. In particular, the regular potential in Ω_s is larger than the total potential φ by $\varepsilon_s/\varepsilon_m \approx 40$ times. Consequently, when the numerical solution of φ^h is added to the analytical solution of φ^s to get the total potential, the relative numerical error will be amplified by about 40 times. For this reason we will apply a stable decomposition to the PNP equations in this study. This decomposition is first introduced by Chern *et. al.* for solving the Poisson-Boltzmann equation with an interface method [13].

We define the singular component φ^s to be the restriction on Ω_m of the solution of

$$-\varepsilon_m \Delta \varphi^s(x) = \rho^f(x), \quad x \in \mathbb{R}^3,$$

(7)

and the harmonic component $\varphi^h(x)$ to be the solution of a Laplace equation:

$$-\Delta \varphi^h(x) = 0, \quad x \in \Omega_m,$$
$$\varphi^h(x) = -\varphi^s(x), \quad x \in \Gamma.$$

(8)

It is seen that $\varphi^s(x)$ can be given analytically by the sum of Coulomb potentials. This $\varphi^s(x)$ is then used to compute the boundary condition for $\varphi^h(x)$, the latter is to be solved numerically from Eq. (8), for which we use a finite element method in this study. Subtracting these two components from Eq. (2) we get the governing equation for the regular component $\varphi^r(x)$:

$$-\nabla \cdot (\varepsilon \nabla \varphi^r(x,t)) - \lambda \sum_i q_i \rho_i(x,t) = 0, \quad r \in \Omega,$$

(9)

and the interface conditions

$$\varphi_s^r - \varphi_m^r = 0, \qquad \varepsilon_s \frac{\partial \varphi_s^r}{\partial n} - \varepsilon_m \frac{\partial \varphi_m^r}{\partial n} = \varepsilon_m \frac{\partial (\varphi^s + \varphi^h)}{\partial n}, \qquad x \in \Gamma.$$

(10)

It is worth noting that there is no decomposition of the potential in the solvent region, thus $\varphi(x) = \varphi^r(x)$ in Ω_s. Hence the final regularized Poisson-Nernst-Planck equations consist of the regularized Poisson equation (9) and

$$\frac{\partial \rho_i(x)}{\partial t} = \nabla \cdot D_i(x) \left(\nabla \rho_i(x) + \beta q_i \rho_i(x) \nabla \varphi^r(x) \right), \qquad x \in \Omega_s.$$

(11)

To simplify the presentation we use φ to denote the electrostatic potential coupled with the Nernst-Planck equation, but keep in mind that the singular and harmonic components are to be added to get the full potential inside molecules.

Compared to the original model (1–3), the regularized PNP equations (7–10) has a number of nice properties. First, the decomposition of electrostatic potential occurs only inside biomolecules, thus the numerical solution of φ^r in Ω_s does not suffer the instability [27]. Second, the singular and harmonic components only need to be solved one time *a priori* the coupled solutions of the regularized PNP equations. Indeed, it is the regular potential in solvent region that couples the Nernst-Planck equation and the regular Poisson equation. The singular and harmonic components serve only for providing a fixed interface conditions for solving the regular component, which varies with the ionic concentrations. Noticing that the harmonic component satisfies a Laplace equation, its numerical solution could be further accelerated by taking advantage of various fast numerical methods for boundary integral equations.

We apply the following boundary conditions for the PNP equations. The approximate Debye law is used to compute the value of $\varphi^r = \varphi$ on the exterior boundary $\partial \Omega$:

$$\varphi(x) = \sum_j \frac{q_j e^{-\kappa |x - x_j|}}{\varepsilon_s |x - x_j|},$$

where $\kappa = 1/\lambda_d^2$ with λ_d being the Debye length computed from the bulk concentrations of all species of charged particles. For all species of particles ρ_i on $\partial \Omega$ is given by its bulk concentration. A zero macroscopic normal flux

$$D_i(\nabla \rho_i + \beta q_i \rho_i \nabla \varphi) \cdot n = 0$$

is prescribed on the non-reactive molecular surface $\Gamma \backslash \Gamma_a$ with outer normal vector n for all species. For particles that react with the molecule on the surface Γ_a we apply the homogeneous Dirichlet boundary condition, i.e., $\rho_i = 0$. This models the fact that the diffusion time scale is much larger than the reactive time scale, and that in the solution there is a sufficient large number of solute molecules which are able to hydrolyze all ligands that migrate to the reaction centers of solute molecules. The non-zero flux on the reactive surface makes the particle concentrations described by PNP differ fundamentally from the Boltzmann distribution, which can be reproduced if the macroscopic flux is vanishing

everywhere [45]. As we shall see, reactive molecular surface and multiple species of charged particles make the solution near the surface far from electrically neutral. This might prevent us from using alternative elliptic equation for describing the electrostatics that relies on the electroneutrality condition [39].

3. Computational Algorithms

The numerical methods we shall develop and analyze are focused at three major aspects of the PNP model: the self-adjointness of the elliptic operator in NP equation; the nonlinearity of the system due to the drift term; and the coupling between Poisson and NP equations for both steady and unsteady diffusions.

3.1. Self-adjointness of the electro-diffusion operator

It is known that by introducing the Slotboom variables

$$\overline{D}_i = D_i e^{-\beta q_i \varphi}, \quad \overline{\rho}_i = \rho_i e^{\beta q_i \varphi},$$

(12)

the Nernst-Planck equation can be transformed to be

$$\frac{\partial(\overline{\rho}_i e^{-\beta q_i \varphi})}{\partial t} = \nabla \cdot (\overline{D} \nabla \overline{\rho}).$$

(13)

These transformations, frequently used in solving the PNP equations for semiconductor device simulations [4,28], hence give rise to a self-adjoint, uniformly elliptic operator in case of a fixed potential. It is anticipated that the discretization in solving the transformed equation (13) could produce a stiffness matrix with a smaller condition number compared to the original equation (11) with a non-symmetric elliptic operator, and thus iterative methods applied to the linear system might converge faster. Although this expectation seems reasonable, a large variation of the potential on the molecular surface is often seen because of the fixed charges of different signs inside molecules. Consequently, the transformed diffusion coefficient $\overline{D}$ could vary drastically from its maximum to the minimum, hence the actual condition number of the stiffness matrix for the self-adjoint formulation (13) may be not as small as we anticipate. Moreover, the application of transformations (12) to the electrostatic Poisson equation (9) will lead to

$$-\nabla \cdot (\varepsilon \nabla \varphi) - \lambda \sum_i q_i \overline{\rho}_i e^{-\beta q_i \varphi} = 0.$$

(14)

The corresponding operator is thus no longer self-adjoint in contrast to the equation (9). While the equation (14) appears identical to the nonlinear Poisson-Boltzmann equation, the actual particle concentrations, nevertheless, do not follow the Boltzmann distribution if there is a non-zero macroscopic flux inside the domain or on the boundary. In the next section we shall numerically compare the primitive asymmetric and transformed self-adjoint formulations of the steady-state Nernst-Planck equation with regard to the condition number of the respective stiffness matrix.

It is worth noting that the Slotboom variables are associated with the weighted inner product in many finite element approximations of semiconductor NP equations [19], for which

exponential fitting techniques are usually used to obtain numerical solutions free of non-physical spurious oscillations. Although the solutions in our numerical experiments and biophysical applications presented below do not show significant non-physical oscillations, these methods can be adopted if needed.

3.2. Steady-state diffusion

We first consider the finite element solution of the steady state PNP equations (9,11). To this end we define the solution space

$$H := \{(\varphi, \rho) \in H_0^1(\Omega) \times H_{0_1}^1(\Omega_s) \times \cdots H_{0_n}^1(\Omega_s)\} \tag{15}$$

and its finite dimensional subspace

$$S := \{(\varphi, \rho) \in P_1(\Omega) \times (P_1(\Omega_s))^n\}, \tag{16}$$

where the vector $\rho = \{\rho_j\}_{j=1}^n$, and P_1 is the space consisting of piecewise linear tetrahedral finite elements. Functions in the space

$$H_{0_i}^1 = \{v \in H^1(\Omega_s): v=0 \; on \; \partial\Omega, \; v=0 \; on \; \Gamma_{D_i}\}$$

satisfy the Dirichlet boundary condition on the exterior boundary $\partial\Omega$ and the essential or Dirichlet boundary condition on the molecular surface Γ if there is one. We assume that the finite elements are regular and quasi-uniform. The weak formulation of the problem now is:

Find u = (φ, ρ) ∈ S such that

$$\langle F(u), v \rangle = 0, \quad \forall v = (\psi, \eta) \in S. \tag{17}$$

Here the nonlinear mapping $F : H \mapsto H^*$ and $\langle \cdot, \cdot \rangle$ is the standard duality paring between the dual space H^* and H. Specifically, the nonlinear weak form $\langle F(u), v \rangle$ is defined to be

$$\langle F(u), v \rangle = \begin{bmatrix} (\varepsilon\nabla\varphi, \nabla\psi) - (\lambda\sum_i q_i\rho_i, \psi) + \langle p, \psi \rangle_\Gamma \\ (D_i\nabla\rho_i, \nabla\eta_i) + (D_i\beta q_i\rho_i\nabla\varphi, \nabla\eta_i) \end{bmatrix}, \tag{18}$$

where

$$p = \varepsilon_m \frac{\partial(\varphi^s + \varphi^h)}{\partial n}$$

is the jump in electric displacement defined in Eq. (10), $\langle \cdot, \cdot \rangle_\Gamma$ denotes the L_2 inner product defined on the interface Γ, and the L_2 scalar inner product over the domain Ω or Ω_s is denoted by $(\cdot, \cdot)$. To solve the nonlinear problem (17) we employ the damped inexact-

Newton method [26] which necessitates the Gâteaux derivative $DF(u)$ defined by the bilinear form

$$\langle DF(u)w, v\rangle = \frac{d}{d\tau}\langle F(u+\tau w), v\rangle|_{\tau=0}$$
$$= \begin{bmatrix} (\varepsilon\nabla\phi, \nabla\psi) - (\lambda\sum_i q_i\varrho_i, \psi) \\ (D_i\nabla\varrho_i, \nabla\eta_i) + D_i\beta q_i(\rho_i\nabla\phi + \varrho_i\nabla\varphi, \nabla\eta_i) \end{bmatrix} \tag{19}$$

where $w = (\phi, \varrho)$. With these well-defined operators the complete algorithm can be given as follows:

Algorithm 3.1

- Choose the initial approximation u = (φ, ρ), the nonlinear tolerance ε, the residual r in approximately solving the linear system, and the damping factor λ.

- Do until $|\langle F(u), v\rangle| < \varepsilon$

    1. Solve the correction w from $\langle DF(u)w, v\rangle = -\langle F(u), v\rangle + r$.

    2. $u \Leftarrow u + \lambda w$.

A constant damping parameter $\lambda = 1$ is chosen in this study, with which the convergence is reached in less than 20 steps in all simulations.

We also consider the finite element solution of transformed PNP equations (13,14). For which the solution $u = (\varphi, \bar{\rho})$ contains the transformed particle concentrations and nonlinear weak form $\langle F(u), v\rangle$ is given by

$$\langle F(u), v\rangle = \begin{bmatrix} (\varepsilon\nabla\varphi, \nabla\psi) - (\lambda\sum_i q_i\bar{\rho}_i e^{-\beta q_i\varphi}, \psi) + \langle p, \psi\rangle_\Gamma \\ (\overline{D}_i\nabla\bar{\rho}_i, \nabla\bar{\eta}_i) \end{bmatrix}, \tag{20}$$

where $v = (\psi, \bar{\eta})$. Accordingly, the bilinear form now is

$$\langle DF(u)w, v\rangle = \frac{d}{d\tau}\langle F(u+\tau w), v\rangle|_{\tau=0}$$
$$= \begin{bmatrix} (\varepsilon\nabla\phi, \nabla\psi) - (\lambda\sum_i(q_i\bar{\varrho}_i - \beta q_i^2\bar{\rho}_i\varphi)e^{-\beta q_i\phi}, \psi) \\ (\overline{D}_i(\nabla\bar{\varrho}_i + \beta q_i\phi\nabla\bar{\rho}_i), \nabla\bar{\eta}_i) \end{bmatrix} \tag{21}$$

where $w = (\phi, \bar{\varrho})$. The complete algorithm for solving the transformed PNP equations is the same as Algorithm (3.1) but with $\langle F(u), v\rangle$ and $\langle DF(u)w, v\rangle$ defined by (20) and (21), respectively. It is worth noting that the operator $DF(u)w$ defining the linearized equation for solving correction variable w is not self-adjoint regardless of the transformation due to the nonlinearity of the PNP model.

3.3. Unsteady-state diffusion

For time-dependent problems the elliptic equation for the electrostatic potential and parabolic equations for the particle concentrations are solved sequentially. The weak form of the unsteady Nernst-Planck equation for i-th species of particle is

$$\langle F(\rho_i), v\rangle = \int_{\Omega_s} \left[D_i(\nabla\rho_i + \beta q_i\rho_i\nabla\varphi^r) \cdot \nabla v + \frac{\partial\rho_i}{\partial t}v \right] dx, \forall v \in H^1_{0_i}(\Omega_s). \tag{22}$$

Various schemes can be used for the time discretization of this equation. For example, Prohl and Schmuck proposed convergent schemes based on different types of fixed-point mappings [43]. Due to the nonlinearity of the equation, the application of these and high order methods such as a third-order Runge-Kutta method or its combination with the exponential time differencing (ETD) method [15,36] demands solving the electrostatic potential multiple times in each step of time evolution. To reduce the computational cost and maintain the stability, we adopt the Crank-Nicolson method for the time discretization. This gives rise to the following semi-discrete equation at $t_{n+1/2}$ for $n > 0$:

$$\langle F(\rho_i^{n+1/2}), v\rangle = \int_{\Omega_s} \left[D_i\left(\nabla\frac{\rho_i^{n+1}+\rho_i^n}{2} + \beta q_i\frac{\rho_i^{n+1}+\rho_i^n}{2}\nabla\varphi^{n+1/2} \right) \cdot \nabla v + \frac{\rho_i^{n+1}-\rho_i^n}{\Delta t}v \right] dx \tag{23}$$

for a constant time increment Δt. Here the electrostatic potential $\varphi^{n+1/2}$ is solved from the Poisson equation (9) with particle concentrations at $t_{n+1/2}$ computed with an Adams-Bashforth scheme

$$-\nabla \cdot \left(\varepsilon\nabla\varphi^{n+1/2}\right) - \lambda\sum_i q_i\frac{3\rho_i^n - \rho_i^{n-1}}{2} = 0. \tag{24}$$

We then use the inexact-Newton approach presented above to solve ρ_i^{n+1} from the equation

$$\langle F(\rho_i^{n+1/2}), v\rangle = 0. \tag{25}$$

To this end we need the Gâteaux derivative $DF(\rho_i^{n+1})$, which is now defined by

$$\langle DF(\rho_i^{n+1/2})w, v\rangle = \frac{d}{d\tau}\langle F(\rho_i^{n+1/2}+\tau w), v\rangle|_{\tau=0}$$
$$= \int_{\Omega_s} \left[\frac{1}{2}D_i\left(\nabla w \cdot \nabla v + \beta q_i w\nabla\varphi^{n+\frac{1}{2}}\right) + \frac{w}{\Delta t}v \right] dx, \tag{26}$$

where $w \in H^1_{0_i}$. The solutions of (25)–(26) follow Algorithm (3.1) with residual $r = 0$. Since equation (23) is linear in ρ_i^{n+1}, only one solution of w is needed for an arbitrary initial guess of ρ_i^{n+1} at each time step. The application of the inexact-Newton method here makes it easy to modify the computer codes developed for this linear problem to solve the nonlinear Nernst-Planck equations with finite particle sizes, such as that in [32]. We note that a similar Adams-Bashforth-Crank-Nicolson (ABCN) method was used for solving the Navier-Stokes equations and ensuring divergence-free velocity field [44,53]. The extrapolation of source term at t_n, t_{n-1} in Eq. (24) is similar to the construction of the pressure Poisson equation at $t_{n+1/2}$ in those studies.

3.4. Finite element implementation and mesh generation

The numerical implementation of Algorithm (3.1) for solving Eq. (17), Eq. (25) and the Poisson equation (24) is carried out using FETK, an expandable collection of the adaptive finite element method (AFEM) software libraries [25]. Standard linear finite element spaces and Galerkin approximation are adopted in these solutions.

The mesh generation technique for the solvated biomolecular system is similar to that described in our former work [35]. We start with a triangulated molecular surface mesh generated by MSMS [46]. This initial surface mesh is then processed to remove the degenerate triangles and improve the regularity and uniformity of the mesh. The improved surface mesh and the spherical exterior boundary mesh are supplied to TETGEN [48] to finally generate a quality tetrahedral mesh through adaptive 3-D delaunay triangulation. While the Poisson equation and the NP equations are solved in different domains, only one file of the mesh in the entire Ω and conforming to Γ is input to FETK. The mesh of $\bar{\Omega}_s$ is extracted by a subprogram.

4. Numerical Experiments and Biophysical Applications

4.1. Conditioning of the Nernst-Planck equation

The elliptic operator in the transformed Nernst-Planck equation (13) is self-adjoint but its advantages in the numerical solution over the primitive formulation remain to be shown. Here we shall examine the conditioning of the stiffness matrices resulting from the discretization of the two elliptic equations

$$\nabla \cdot (D_i \nabla \rho_i + D_i \beta q_i \rho_i \nabla \varphi) = 0, \tag{27}$$

$$\nabla \cdot (\overline{D}_i \nabla \overline{\rho}_i) = 0, \tag{28}$$

where $\overline{D}$ and $\bar{\rho}$ are defined in (12). The function φ is chosen to be the electrostatic potential induced by a charged unit sphere, i.e.,

$$\varphi = Q/(\varepsilon_s r),$$

where Q is the charge located at the center of the sphere and r is the distance to the center. We consider the diffusion of a single species of particles in the spherical annulus Ω_s between $r = 1$ and $r = 4$, with various boundary conditions on the surface of the unit sphere. The magnitude of the potential φ is varied by adjusting the singular charge Q. We note that this potential is given and is not consistent with the particle concentration. The condition numbers of the sparse stiffness matrices are computed by using the MATLAB function *condest*.

Fig. (2) plots the variation of the condition number of the stiffness matrix for two formulations with different charge Q and boundary conditions on $r = 1$. It it obvious that the transformed formulation is related to a larger condition number for all combination of boundary conditions and particle charges. Indeed, the stiffness matrix $\overline{A}$ for the transformed Nernst-Planck equation (28) is

$$\overline{A}=\Lambda A=\mathrm{diag}\left(e^{-\beta q\varphi_{p_1}},e^{-\beta q\varphi_{p_2}},\cdots,e^{-\beta q\varphi_{p_n}}\right)A \tag{29}$$

where A is the stiffness matrix for the Laplace equation $-\nabla\cdot(D\nabla\bar{\rho})=0$, and diag $(\cdot)$ is the diagonal matrix. φ_{p_j} is the electrostatic potential at the jth node of the mesh in Ω_s, and is positive in our problem since $Q>0$. The condition number of A is determined by the discretization of Ω_s and the finite element space used, and is independent of the permanent charge Q and the potential φ. We then have the following estimate for the upper bound of the condition number of $\bar{A}$:

$$\begin{aligned}k(\overline{A})&=\left\|\Lambda A\right\|\cdot\left\|(\Lambda A)^{-1}\right\|\le\left(\left\|\Lambda\right\|\cdot\left\|\Lambda^{-1}\right\|\right)\left(\left\|A\right\|\cdot\left\|A^{-1}\right\|\right)\\&\le k(\Lambda)k(A)=\frac{\max_{p_j}\{e^{-\beta q\varphi_{p_j}}\}}{\min_{p_j}\{e^{-\beta q\varphi_{p_j}}\}}k(A).\end{aligned} \tag{30}$$

Because of the inverse proportional decay of the potential φ with the distance r, the exponential factor $e^{-\beta q\varphi}$ varies significantly from the sphere surface to the exterior boundary. Consequently, if the diffusive particles carry negative unit charge, the exponential factor near the unit sphere will be very large compared to that close to the exterior boundary. In other words,

$$\frac{\max_{p_j}\{e^{-\beta q\varphi_{p_j}}\}}{\min_{p_j}\{e^{-\beta q\varphi_{p_j}}\}}=\frac{e^{\beta Q/\varepsilon_s}}{e^{\beta Q/(4\varepsilon_s)}}, \tag{31}$$

suggesting the condition number of the stiffness matrix will be large. Similarly, if the diffusion particles carry unit positive charge, the exponential factor near the unit sphere will be very small compared to that close $\partial\Omega$, i.e.,

$$\frac{\max_{p_j}\{e^{-\beta q\varphi_{p_j}}\}}{\min_{p_j}\{e^{-\beta q\varphi_{p_j}}\}}=\frac{e^{-\beta Q/(4\varepsilon_s)}}{e^{-\beta Q/\varepsilon_s}}, \tag{32}$$

indicating that the condition number of the matrix will be large also. The exponential growth of above two ratios with Q will cause a correspondingly growth of the condition number for large permanent charge as seen in the charts C and D.

The partial charge carried by any atom in a biomolecule is generally smaller than 2 (i.e., two fold of the elementary charge), suggesting that we do not have large Q in most real biophysical problems. But the ratio in Eq. (30) can still be extremely large if there are positive and negative permanent charges presented inside biomolecules. To prove this numerically we choose φ to be the electrostatic potential induced by a molecule comprising of two unit spheres located at $(1.5, 0, 0)$ and $(-1.5, 0, 0)$ respectively. A solvent probe of radius of 1.4 is chosen and thus the molecular surface is formed by two spherical caps connected by a circular reentrant surface. The left sphere carries a charge Q at its center while the right one carries a charge $-Q$. The radius of the exterior sphere is 4. Fig. (3) shows the distribution of φ for $Q = 2$ on the $x - y$ plane and on the surface of molecule. It is seen that $\varphi_{\max} > 5$ and $\varphi_{\min} < -5$, and hence

$$\frac{\max_{p_j}\{e^{-\beta q\varphi_{p_j}}\}}{\min_{p_j}\{e^{-\beta q\varphi_{p_j}}\}} > \frac{e^{5\beta}}{e^{-5\beta}} = 1.9269 \times 10^7,$$

(33)

assuming that $q = \pm 1$ and a value $\beta = 1.6774$ at room temperature $T = 300K$. This justifies the quick growth of the condition number for the transformed formulation as shown in Fig. (4). Since any biomolecule carries both positive and negative charges, the transformed formulation will always lead to an ill-conditioned stiffness matrix. For this reason we shall use the primitive formulation in all the following computations. It is also seen that the reactive boundary condition is always associated with a smaller condition number than the non-reactive boundary condition. We note that the transformation with Slotboom variables is associated with the weighted inner product in many finite element approximations of semiconductor NP equations [19]. Exponential fitting techniques or other up-winding techniques are usually necessary for obtaining numerical solutions free of non-physical spurious oscillations. Although the solutions in our numerical experiments and biophysical applications presented below do not show significant non-physical oscillations, these stabilization methods can be adopted if needed.

4.2. Steady-state diffusion: numerical accuracy and electroneutrality

Due to the intrinsic nonlinearity of the equation, the analytical solutions for the steady-state PNP equations are not available in general, even for the simplest problems such as the electrodiffusion in the spherical annulus exterior to a charged sphere. Here we choose two examples to examine the accuracy of our algorithm. The first example is to solve the Nernst-Planck system for the concentration of a single species at a given potential $\varphi(r) = Q/(\varepsilon_s r)$ in a spherical annulus:

$$-\frac{1}{r^2}\frac{d}{dr}\left(r^2 D\left(\frac{d\rho}{dr} - \beta\rho q\frac{Q}{\varepsilon_s r^2}\right)\right) = 0, \, r_1 < r < r_2$$
$$\rho(r_1) = 0, \rho(r_2) = \rho_0,$$

(34)

where ρ_0 is the bulk concentration. Note here we are applying a reactive boundary condition on the whole sphere $r = r_1$. The analytical solution for Eq. (34) is

$$\rho(r) = \rho_0 \frac{e^{-\beta w(r)} - e^{-\beta w(r_1)}}{e^{-\beta w(r_2)} - e^{-\beta w(r_1)}}, \text{ where } w(r) = \frac{qQ}{\varepsilon_s r}.$$

(35)

The reactive rate constant k_r is then computed from the flux $J(r)$ on the reactive surface via

$$-k_r \equiv \frac{\int_{S_A} J(r)ds(r)}{\rho_0} = \frac{4\pi r_1^2 J(r_1)}{\rho_0} = 4\pi D w(r_1)r_1 \frac{-e^{-\beta w(r_1)}}{e^{-\beta w(r_2)} - e^{-\beta w(r_1)}}$$

(36)

where S_A is the reactive surface. In this case we choose $r_1 = 1$, $r_2 = 40$, $\varepsilon_s = 78\varepsilon_0$, $\rho_0 = 50mM$, $D = 78000\text{Å}/\mu s$, $q = -1$, $Q = 1$, and thus the exact $k_r = 2.5315 \times 10^{11} M^{-1} min^{-1}$. Table (1) lists the relative L_2 errors of the computed particle concentration, the asymptotic order of error reduction and the reaction rate constants. These results demonstrate that our finite element method is convergent for this problem, with an asymptotic rate of convergence close to 2 as anticipated for a linear finite element method. It is also noticed

that the errors in the computed reactive rate constant are large for all the mesh sizes considered. This is related to the very large gradient of concentration close the reactive surface, as seen in Fig. (5) where the exact and computed concentration profiles are plotted. Physically, this large gradient is induced by the electrostatic attraction of the negatively charged particles to the positively charged sphere. In this study we use finite element meshes refined toward the molecular surface to improve the local numerical resolution. Other higher order methods can also be introduced to this problem to resolve this large gradient and improve the numerical accuracy.

The second example is to solve the full steady-state PNP equations for two species of particles, one carries charge −1 and the other has charge +1, in the same spherical annulus as in the last example. We prescribe the flux $J(r) = 0$ for both species on the unit sphere, and the particle concentrations on the exterior boundary are set to be the respective bulk concentrations. The macroscopic flux of either species of particles is therefore zero everywhere in the domain, and thus the PNP model shall produce the nonlinear Poisson-Boltzmann equation and the particle concentrations shall follow the Boltzmann distribution. This criterion is used to examine the numerical solutions of the PNP equations. We would note that there is no analytical solution of the potential available for the nonlinear Poisson-Boltzmann equation. Rather, we will compare the computed concentration profiles of the PNP equations and those predicted by using the Boltzmann distribution and the computed electrostatic potential. In particular, let the numerical solutions of the potential and the particle concentration be φ and ρ, and the exact solutions of them be $\hat{\varphi}$ and $\hat{\rho}$, respectively. Let the particle concentration computed from the solved potential φ be $\tilde{\rho}$, then the error we are measuring is $\rho - \tilde{\rho}$. It follows that for any Sobolev norm $\| \cdot \|$ we have

$$
\begin{aligned}
\left\| \rho - \tilde{\rho} \right\| &\le \left\| \rho - \widehat{\rho} \right\| + \left\| \widehat{\rho} - \tilde{\rho} \right\| \\
&= \left\| \rho - \widehat{\rho} \right\| + \left\| \rho_0 e^{-q\beta\widehat{\varphi}} - \rho_0 e^{-q\beta\varphi} \right\| \\
&\le \left\| \rho - \widehat{\rho} \right\| + \left\| \rho_0 e^{-q\beta\widehat{\varphi}} \right\|_\infty \left\| e^{-q\beta(\varphi - \widehat{\varphi})} - 1 \right\| \\
&\approx \left\| \rho - \widehat{\rho} \right\| + \left\| \rho_0 e^{-q\beta\widehat{\varphi}} \right\|_\infty \left\| q\beta(\varphi - \widehat{\varphi}) \right\| \\
&= \left\| \rho - \widehat{\rho} \right\| + C \left\| \varphi - \widehat{\varphi} \right\|,
\end{aligned}
\tag{37}
$$

where the constant C is independent of the numerical methods. This estimate suggests that the error we are measuring has the same rate of convergence as the error of solutions of the PNP equations. Tab. (2) shows that the rate with respect to L_2 norm is about 1, which is close to the one predicted for the linear elliptic interface problems in [12]. Fig. (6) plots the computed particle concentration and that predicted by the Boltzmann distribution. The flattening of the profile close to $r = 1$ indicates the vanishing concentration due to the electrostatic repulsion and the vanishing macroscopic flux as prescribed by the boundary condition.

We move to the investigation of the electroneutrality and its relation to the boundary conditions. For this purpose we first consider three diffusion problems in the spherical annulus $1 \le r \le 40$: (1) $50mM:50mM$ symmetrical solution without reaction on sphere; (2) $50mM:50mM$ symmetrical solution with the negatively charged particles reactive on sphere; and (3) $50mM:25mM:25mM$ asymmetrical solution with the third species of particle reactive on sphere. Here the ratios refer to the bulk concentrations of particles. In the third problem the first species of particles is positively charged and the other two are negatively charged. The computed net charge concentration

$$q_{net}(r) = \sum_i q_i \rho_i$$

is plotted in Fig. (7) for all three solutions.

Chart A shows that near the reactive surface the net charge concentration is close to zero. This is a result of the depletion of positively charged particle due to the electrostatic repulsion and the depletion of negative charged particle due to the reaction boundary conditions $\rho_i = 0$. On the other hand, the electrostatic attraction causes the aggregation of the negatively charged particles toward the sphere, as can be seen at the peak of excessive negative charges. The balance of oppositely charged particles are gradually built with the increase of distance to the unit sphere. If the negatively charged particles are non-reactive, these particles will aggregate near the unit sphere, which in turn gives rise to a large concentration of negative charged particles as shown in the blue profiles in Chart B. If only a part of the negatively charged particles are reactive, very large concentration of the non-reactive negatively charged particles is still seen in the red profile of the chart B. It it also seen that the two profiles in Chart B are very close, suggesting that part of the negatively charged particles being reactive does not significantly change the electroneutrality of the solution. This is not surprising since the non-reactive negatively charged particles can still be attracted to the sphere to generate a large concentration.

Noticing that the observations above are made from the solutions of different problems, we now consider a model problem defined in the spherical annulus $1 \le r \le 4$ with both reactive and nonreactive boundary conditions, on $r = 1$, as shown in Fig. (8). The unit sphere with a unit positive charge at its center models the molecular surface. The reactive boundary is the spherical cap to the right of the plane $x = 0.9165$, and the remaining spherical surface is nonreactive. We consider a 1:1 symmetric solution with bulk concentrations being $50mM$. Fig. (8) features the aggregation of the negatively charged particles on the nonreactive molecular surface as well as the depletion of these particles on the reactive surface. The net charge concentration along x-axis is plotted in Fig. (9), where in the right chart we observe the neutrality close to $x = 1$ due to the reactive boundary condition and the peak of the excessive negative charge. We also compute the problem with a $2 : 1 : 1$ solution defined as above. The appearance of non-reactive negative charges completely changes the neutrality close to $x = 1$, since these charges will be attracted to the entire surface including the reactive surface and aggregate. Consequently for $x \in [1,4]$ we shall observe a profile similar to the left chart of Fig. (9). In a biological solution there are many species of non-reactive particles carrying charges of the same sign as the reactive particles, and therefore a large concentration near the charged molecular surface is always present.

4.3. Accuracy for solving the unsteady-state diffusion

To examine the accuracy of the time integration method we design a problem that has the essential features of the PNP and admits an analytical solution:

$$-\nabla \cdot (\varepsilon_s \nabla \varphi) = q\rho + f(r), \tag{38}$$

$$\frac{\partial \rho}{\partial t} = \nabla \cdot (D\nabla \rho + \beta q \rho \nabla \varphi) + g(r). \tag{39}$$

This equation is solved in the spherical annulus $1 \leq r \leq 4$. The analytical solutions for φ and ρ are prescribed to be

$$\varphi = \frac{r^2}{\varepsilon_s} e^{-\delta t},$$

(40)

$$\rho = \rho e^{-\beta q r^2 / \varepsilon_s} e^{-\delta t}.$$

(41)

These two analytical solutions determine the functions $f(r)$, $g(r)$ and the Dirichlet boundary conditions for both equations. A very fine mesh with 40859 unknowns is used to ensure that the error due to the time discretization is dominant in the numerical approximation. The equations are integrated to $t = 200$ with various time increments Δt and fixed parameter $\delta = 0.01$. The relative L_2 errors are collected in Tab. (3), which features a convergence of approximately second-order for both variables. This agrees with the convergence of the ABCN scheme applied for solving the Navier-Stokes equations [44]. It is worth noting that here we are using large time increments in time integration; the convergence properties we observed in this study agree with the theoretical analysis [24] which proves that the ABCN for time-dependent Navier-Stokes equations is almost unconditionally stable.

4.4. Biophysical applications

Finally we apply the regularized PNP solver to compute the reaction rate constant of neurotransmitter acetylcholine (ACh) at the reaction center of the enzyme acetylcholinesterase (AChE). The steady-state diffusion problems for this has been studied by using the Smoluchowski equation [50] and a hybrid finite element/boundary element method [35,55]. In the latter approach the boundary element method is used to solve the singular component of the electrostatic potential. We treat the ACh molecules as particles with +1 charge. The computation domain is chosen to be a ball with a radius 400Å centered at the geometric center of the AChE molecule. We consider two other species of non-reactive particles, one with +1 charge and the other with −1 charge. The boundary conditions for these two species of particles are therefore $J_i(r) = 0$ on the whole surface of AChE. The reaction center of the AChE is signified in Fig. (10) in red where $\rho_i = 0$ is set for ACh as the reactive boundary conditions, and on the rest surface the $J_i(r) = 0$ is prescribed. The bulk concentrations of all three species of particles are set to be $50mM$. The same mesh as that in [55] is used in this study. The electrostatic potential on the surface of AChE is shown in Fig. (10) along with the surface mesh and a close view of the potential around the reaction center. The surface potential is smooth overall and the negative potential near the reaction center is well reproduced. The reaction rate constant is 1.72×10^{11}, which well matches that computed by using the hybrid finite element/boundary element method [55]. It is seen that the value of electrostatic potential ranges from −10 to 3. This confirms that a large variation of the potential φ can be seen in real solvated biomolecular system and thus the transformed formulation of the Nernst-Planck is inappropriate in real applications because its ill-conditioned stiffness matrix.

5. Conclusions

We have developed a finite element method for solving the Poisson-Nernst-Planck (PNP) equations with permanent charges. The electrostatic Poisson equations is regularized by analytically removing the singular component of the electrostatic potential from the numerical solution. A harmonic component is defined inside biomolecules to partially

compensate the removed singular component such that the remaining electrostatic component is continuous on the molecular surface. This remaining regular component is governed by an elliptic interface problem, with interface conditions computed once only from the singular and the harmonic components. It is shown that the diffusion in the solvent region is completely drifted by the regular component, which gives rise to regularized Poisson-Nernst-Planck equations. An inexact-Newton method was used to solve the regular PNP for steady diffusion. For unsteady diffusion we proposed a second-order Adams-Bashforth-Crank-Nicolson method for time integration. Due to the limited availability of the analytical solutions to 3-D PNP, we constructed various test problems to examine the accuracy and the stability of the proposed finite element methods and time integration scheme.

We numerically compare the usefulness of the primitive and transformed formulations of the Nernst-Planck equation, by studying the conditioning of the associated stiffness matrices. It is shown that the transformed formulation is always related to a large condition number of the stiffness matrix. This can be caused by a large magnitude of the permanent charge, or more generally the existence of both positive and negative charges inside molecules. The primitive formulation of the Nernst-Planck equation is therefore preferred in real simulation although its differential operator is not self-adjoint. Furthermore, we find that given the co-existence of multiple species of charged particles in a biological solution the reactive boundary condition has negligible effects on the electroneutrality of the solution. There are always sufficient nonreactive charged particles being attracted to the reactive surface to generate a high density of net charge. We currently use locally refined mesh to resolve these large gradients of concentrations, while numerical schemes of high resolution are always in demand for this purpose.

It is noticed that the regularized electrostatic Poisson equation appears a Laplace equation inside molecules. This suggests that we can readily map the solution of this Laplace equation to the molecular surface, and eventually cast the regular PNP equations to be integro-differential equations with appropriate Dirichlet-Neumann mapping. The integration of this new formulation with the inexact-Newton approach and the advantage of the overall algorithm are to be explored. In case that the electrodiffusion occurs in solvated system with moving molecules specialized finite element methods could be introduced to solve the equations on a fixed mesh having varying intersections with moving molecular surfaces. Applications of the proposed method to electrodiffusion in real biophysical problems, possibly with effects of finite particle sizes, are also underway.

Acknowledgments

References

1. Abaid, Nicole; Eisenberg, Robert S.; Liu, Weishi. Asymptotic expansions of I-V relations via a Poisson-Nernst-Planck system. SIAM J Appl Dyn Syst 2008;7(4):1507–1526.

2. Baker, NA.; Bashford, D.; Case, DA. Implicit solvent electrostatics in biomolecular simulation. In: Leimkuhler, B.; Chipot, C.; Elber, R.; Laaksonen, A.; Mark, A.; Schlick, T.; Schutte, C.; Skeel, R., editors. New Algorithms for Macromolecular Simulation. Springer; 2006.

3. Baker NA, Sept D, Joseph S, Holst MJ, McCammon JA. Electrostatics of nanosystems: application to microtubules and the ribosome. Proc Natl Acad Sci USA 2001;98:10037–10041. [PubMed: 11517324]

4. Bank RE, Rose DJ, Fichtner W. Numerical methods for semiconductor device simulation. SIAM J Sci Statist Comput 1983;4:416–435.

5. Barcilon V, Chen DP, Eisenberg RS, Jerome JW. Qualitative properties of steady-state Poisson-Nernst-Planck systems: perturbation and simulation study. SIAM J Appl Math 1997;57(3):631–648.

6. Berg, Otto G.; von Hippel, Peter H. Diffusion-controlled macro-molecular interactions. Ann Rev Biophys Biophys Chem 1985;14:131–160. [PubMed: 3890878]

7. Biler, Piotr; Hebisch, Waldemar; Nadzieja, Tadeusz. The Debye system: existence and large time behavior of solutions. Nonlinear Anal 1994;23:1189–1209.

8. Bolintineanu, Dan S.; Sayyed-Ahmad, Abdallah; Davis, H Ted; Kaznessis, Yiannis N. Poisson-Nernst-Planck models of nonequilibrium ion electrodiffusion through a protegrin transmembrane pore. PLoS Comput Biol Jan;2009 5(1):e1000277. [PubMed: 19180178]

9. Brooks BR, Bruccoleri RE, Olafson BD, States DJ, Swaminathan S, Karplus M. CHARMM: A program for macromolecular energy, minimization, and dynamics calculations. J Comput Chem 1983;4:187–217.

10. Cardenas AE, Coalson RD, Kurnikova MG. Three-dimensional Poisson-Nernst-Planck theory studies: influence of membrane electrostatics on gramicidin a channel conductance. Biophys J 2000;79(1):80–93. [PubMed: 10866939]

11. Chen, Long; Holst, Michael; Xu, Jinchao. The finite element approximation of the nonlinear Poisson-Boltzmann equation. SIAM J Numer Anal 2007;45:2298–2320.

12. Chen, Zhiming; Zou, Jun. Finite element methods and their convergence for elliptic and parabolic interface problems. Numerische Mathematik 1998;79(2):175–202.

13. Chern, I-Liang; Liu, Jian-Guo; Wang, Wei-Cheng. Accurate evaluation of electrostatics for macromolecules in solution. Methods Appl Anal 2003;10:309–328.

14. Cohen H, Cooley JW. The numerical solution of the time-dependent Nernst-Planck equations. Biophys J 1965;5:145–162. [PubMed: 14268950]

15. Cox SM, Matthews PC. Exponential time differencing for stiff systems. J Comput Phys 2002;176(2):430–455.

16. Davis ME, Madura JD, Luty BA, McCammon JA. Electrostatics and diffusion of molecules in solution - simulations with the University-of-Houston-Brownian Dynamics program. Comput Phys Commun 1991;62(2–3):187–197.

17. Eisenberg, Bob; Liu, Weishi. Poisson-Nernst-Planck systems for ion channels with permanent charges. SIAM J Math Anal 2007;38(6):1932–1966.

18. Eisenberg R, Chen DP. Poisson-Nernst-Planck (PNP) theory of an open ionic channel. Biophys J 1993;64(2):A22–A22.

19. Gatti E, Micheletti S, Sacco R. A new galerkin framework for the drift-diffusion equation in semiconductors. East-West J Numer Math 1998;6:101–135.

20. Gillespie, Dirk; Nonner, W.; Eisenberg, Robert S. Coupling Poisson-Nernst-Planck and Density Functional Theory to calculate ion flux. J Phys-Condens Mat 2002;14:12129–12145.

21. Gilson MK, Davis ME, Luty BA, McCammon JA. Computation of electrostatic forces on solvated molecules using the Poisson-Boltzmann equation. J Phys Chem 1993;97(14):3591–3600.

22. Gilson MK, Sharp KA, Honig BH. Calculating the electrostatic potential of molecules in solution - method and error assessment. J Comput Chem 1988;9(4):327–335.

23. Graf P, Nitzan A, Kurnikova AG, Coalson RD. A dynamic lattice Monte Carlo model of ion transport in inhomogeneous dielectric environments: method and implementation. J Phys Chem B 2000;104:12324–12338.

24. He, Yinnian; Sun, Weiwei. Stability and convergence of the crank–nicolson/adams–bashforth scheme for the time-dependent navier–stokes equations. SIAM J Numer Anal 2007;45(2):837–869.

25. Holst, M. Finite element toolkit. http://www.fetk.org/

26. Holst M. Adaptive numerical treatment of elliptic systems on manifolds. Adv Comp Math 2001;15(1–4):139–191.

27. Holst M, McCammon JA, Yu Z, Zhou YC, Zhu Y. Adaptive finite element modeling techniques for the Poisson-Boltzmann equation. Commun Comput Phys. 2009 Submitted.

28. Jerome, JW. Analysis of Charge Transport: A Mathematical Study of Semiconductor Devices. Springer; 1996.

29. Jerome, Joseph W. Consistency of semiconductor modeling: an existence/stability analysis for the stationary van Boosbroeck system. SIAM J Appl Math 1985;45:565–590.

30. Jerome, Joseph W.; Kerkhoven, Thomas. A finite element approximation theory for the drift diffusion semiconductor model. SIAM J Numer Anal 1991;28(2):403–422.

31. Kurnikova MG, Coalson RD, Graf P, Nitzan A. A lattice relaxation algorithm for three-dimensional Poisson-Nernst-Planck theory with application to ion transport through the gramicidin a channel. Biophys J 1999;76(2):642–656. [PubMed: 9929470]

32. Li B. Minimization of electrostatic free energy and the Poisson-Boltzmann equation for molecular solvation with implicit solvent. SIAM J Math Anal 2009;40:2536–2566.

33. Liu, Weishi. Geometric singular perturbation approach to steady-state Poisson-Nernst-Planck systems. SIAM J Appl Math 2005;65(3):754–766.

34. Lu B, Zhou YC, Holst M, McCammon J Andrew. Recent progress in numerical solution of the Poisson-Boltzmann equation for biophysical applications. Commun Comput Phys 2008;3:973–1009.

35. Lu BZ, Zhou YC, Huber Gary A, Bond Steve D, Holst Michael J, McCammon JA. Electrodiffusion: A continuum modeling framework for biomolecular systems with realistic spatiotemporal resolution. J Chem Phys 2007;127:135102. [PubMed: 17919055]

36. Lu, Tiao; Cai, Wei. A Fourier spectral-discontinuous Galerkin method for time-dependent 3-D Schrodinger-Poisson equations with discontinuous potentials. J Comput Appl Math 2008;220:588–614.

37. Gilson MK, Sharp K, Honig B. Calculating the electrostatic potential of molecules in solution: Method and error assessment. J Comput Chem 1987;9:327–335.

38. Mori Y, Jerome JW, Peskin CS. A three-dimensional model of cellular electrical activity. Bulletin of the Institute of Mathematics, Academia Sinica 2007;2:367–390.

39. Mori, Yoichiro; Fishman, Glenn I.; Peskin, Charles S. Ephaptic conduction in a cardiac strand model with 3D electrodiffusion. Proc Natl Acad Sci USA 2008;105:6463–6468. [PubMed: 18434544]

40. Nadler B, Schuss Z, Singer A, Eisenberg RS. Ionic diffusion through confined geometries: from Langevin equations to partial differential equations. J Phys-Condens Mat 2004;16(22):S2153–S2165.

41. Nernst W. Die elektromotorische wirksamkeit der ionen. Z Physik Chem 1889;4:129.

42. Planck M. über die erregung von electricität und wärme in electrolyten. Ann Phys Chem 1890;39:161.

43. Prohl, Andreas; Schmuck, Markus. Convergent discretizations for the Nernst-Planck-Poisson system. Numer Math 2009;111(4):591–630.

44. Le Quere P, de Roquefort T Alziary. Computation of natural convection in two-dimension cavities with Chebyshev polynomials. J Chem Phys 1982;57:210–228.

45. Rubinstein, Isaak. Electro-diffusion of Ions. SIAM; 1990.

46. Sanner, Michel F.; Olson, Arthur J.; Spehner, Jean-Claude. Fast and robust computation of molecular surfaces. Proceedings of 11th ACM symposium on computational geometry; 1995. p. C6-C7.

47. Schuss Z, Nadler B, Eisenberg RS. Derivation of Poisson and Nernst-Planck equations in a bath and channel from a molecular model. Phys Rev E 6403(3):2001.

48. Si, H.; Gaertner, K. Meshing piecewise linear complexes by constrained delaunay tetrahedralizations. Proceedings of the 14th International Meshing Roundtable; 2005. p. 147-163.

49. Song YH, Zhang YJ, Bajaj CL, Baker NA. Continuum diffusion reaction rate calculations of wild-type and mutant mouse acetylcholinesterase: adaptive finite element analysis. Biophys J 2004;87(3):1558–1566. [PubMed: 15345536]

50. Song YH, Zhang YJ, Shen TY, Bajaj CL, McCammon JA, Baker NA. Finite element solution of the steady-state Smoluchowski equation for rate constant calculations. Biophys J 2004;86(4): 2017–2029. [PubMed: 15041644]

51. Tai KS, Bond SD, Macmillan HR, Baker NA, Holst MJ, McCammon JA. Finite element simulations of acetylcholine diffusion in neuromuscular junctions. Biophys J 2003;84(4):2234–2241. [PubMed: 12668432]

52. Weiser, Jörg; Shenkin, Peter S.; Still, W Clark. Optimization of Gaussian surface calculations and extension to solvent-accessible surface areas. J Comput Chem 1999;20:688–703.

53. Yang SY, Zhou YC, Wei GW. Comparison of the Discrete Singular Convolution algorithm and the Fourier pseudospectral method for solving partial differential equations. Comput Phys Commun 2002;143:113–135.

54. Zhou YC, Feig Michael, Wei GW. Highly accurate biomolecular electrostatics in continuum dielectric environments. J Comput Chem 2007;29:87–97. [PubMed: 17508411]

55. Zhou YC, Lu BZ, Huber Gary A, Holst Michael J, McCammon JA. Continuum simulations of acetylcholine consumption by acetylcholinesterase - a Poisson-Nernst-Planck approach. J Phys Chem B 2008;112(2):270–275. [PubMed: 18052268]

56. Zhou, Zhongxiang; Payne, Philip; Vasquez, Max; Kuhn, Nat; Levitt, Michael. Finite-difference solution of the Poisson-Boltzmann equation: Complete elimination of self-energy. J Comput Chem 1996;17:1344–1351.
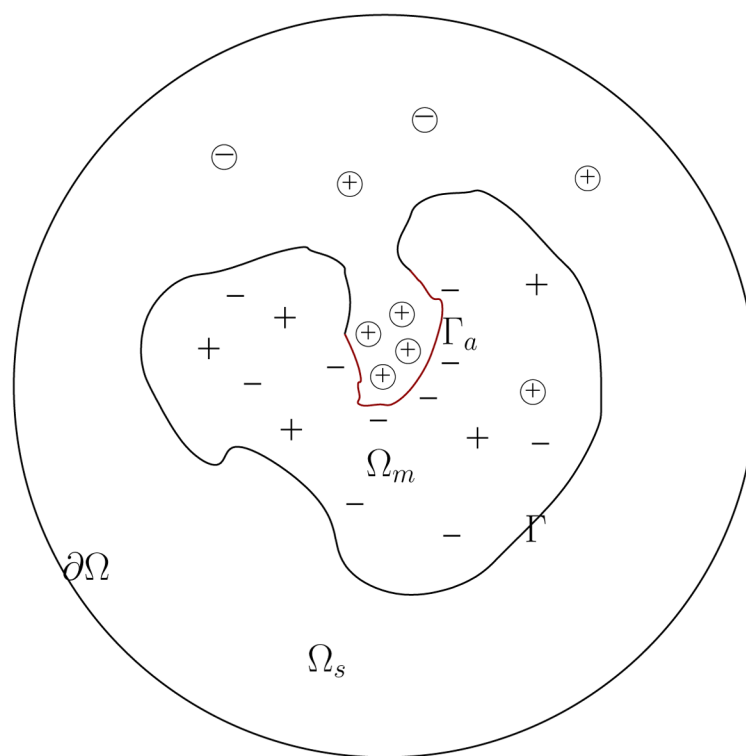
Figure 1.
2-D schematic illustration of the computational domain modeling a solvated biomolecular system. The biomolecule(s) is located in domain Ω_m and the aqueous solution is in domain Ω_s. The molecular surface is Γ. The active reaction center $\Gamma_a \subset \Gamma$ is highlighted in red. The circles with plus or minus sign inside represent the diffusive charged particles which move only in Ω_s. The singular charges inside molecules are signified by plus or minus sign in Ω_m. The minimum distance between the molecular surface Γ and the exterior boundary $\partial\Omega$ is much larger than the diameter of the molecule so that approximate boundary condition for the electrostatics can be applied.
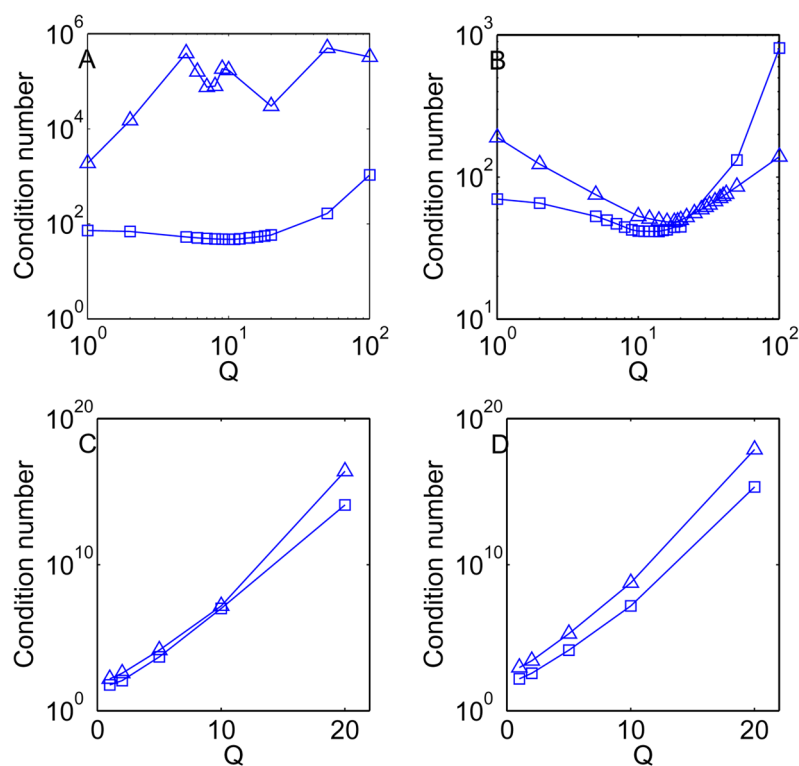
Figure 2.
Change of condition number of the stiffness matrix with the permanent charge Q (in the unit of elementary change). The curves marked with squares are for the reactive boundary condition on the sphere and the curves marked with triangles are for the non-reactive boundary. A: primitive formulation and negatively-charged particle; B: primitive formulation and positively-charged particle; C: transformed formulation and negatively-charged particle; D: transformed formulation and positively-charged particle. More sampling points of the charge Q are used when local extrema of condition number are detected in Chart A and B.
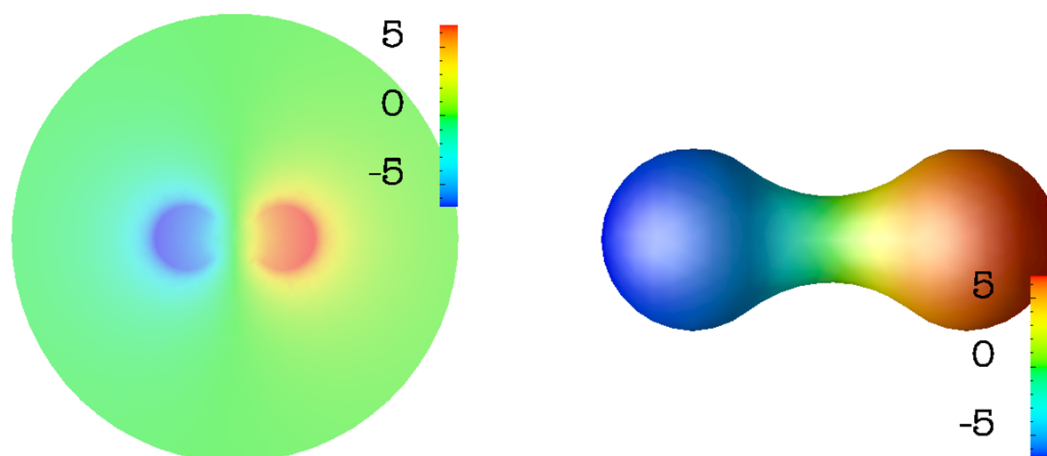
Figure 3.
Electrostatic potential on the $x - y$ plane (left) and on the surface of a model molecule (right).
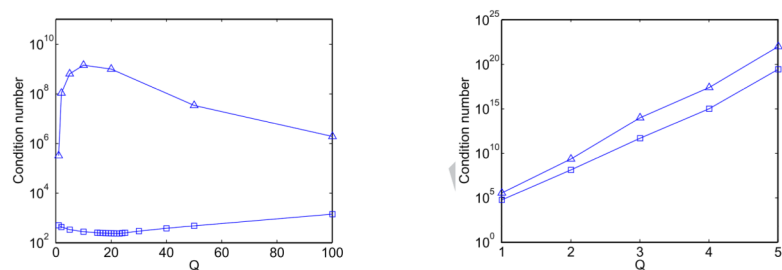
Figure 4.
Change of condition number of the stiffness matrix with the Q(in the unit of elementary change) for the primitive formulation (left) and for the transformed formulation (right). The curves marked with squares are for the reactive boundary condition on the entire molecular surface and the curves marked with triangles are for the non-reactive boundary condition.
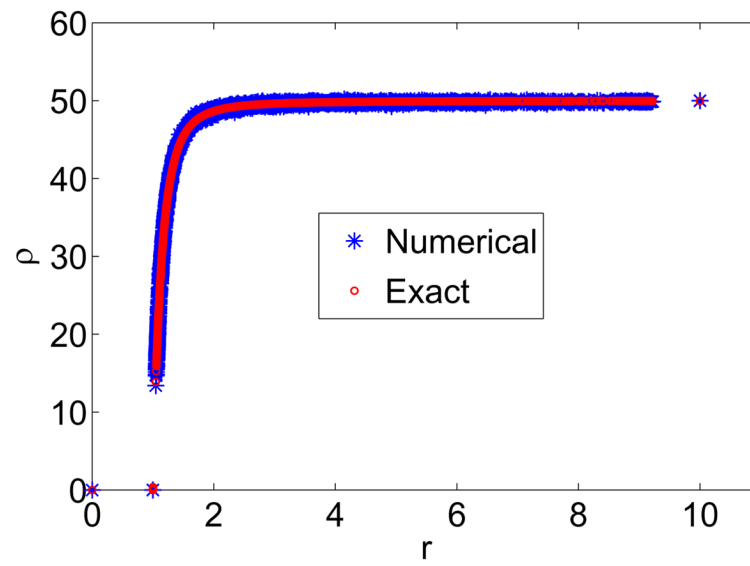
Figure 5.
The exact and computed concentration profiles for the Nernst-Planck equation in the spherical annulus $1 < r < 40$ for a given potential. The *x*-axis is truncated at $r = 10$ in the illustration. $h_{max} = 3.277$.
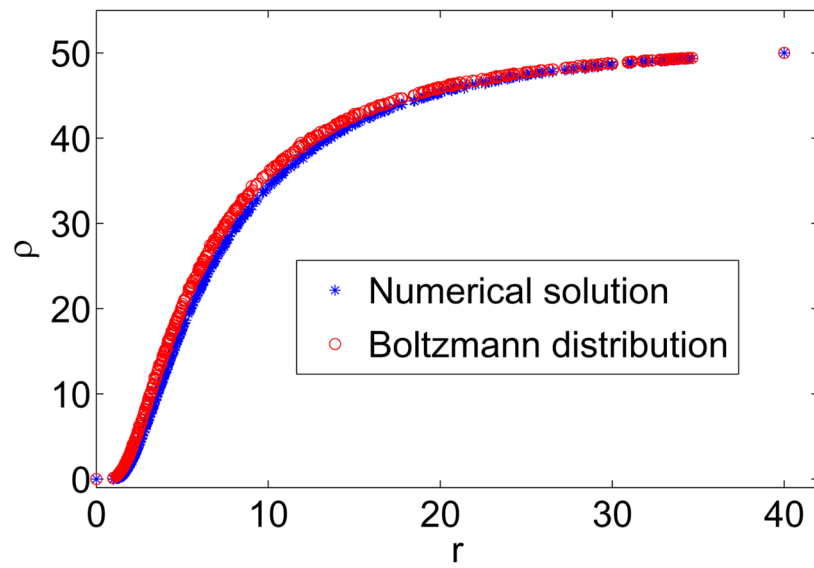
Figure 6.
Computed concentration profiles and the Boltzmann distribution for particles with $q = 1$. $h_{max} = 3.277$.
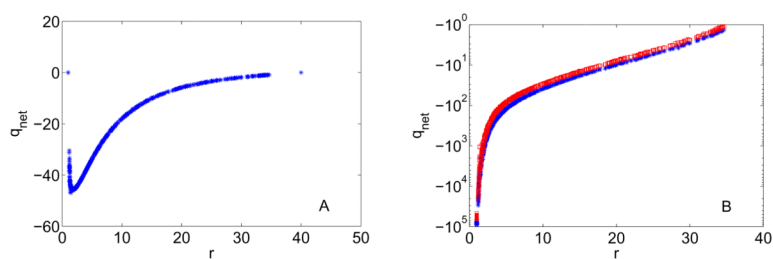
Figure 7.
Profiles of net charge concentrations in *mM*(milli-mol/L) for three solutions. A: symmetrical solution with reactive negatively charged particles; B: symmetrical solution without interaction (blue) and 2:1:1 asymmetrical solution (red).
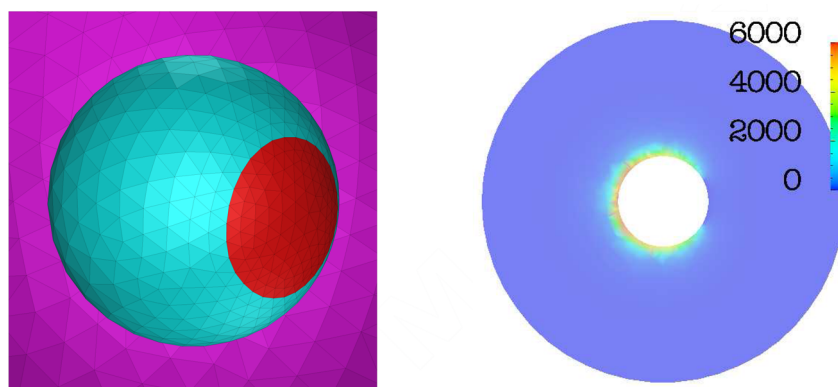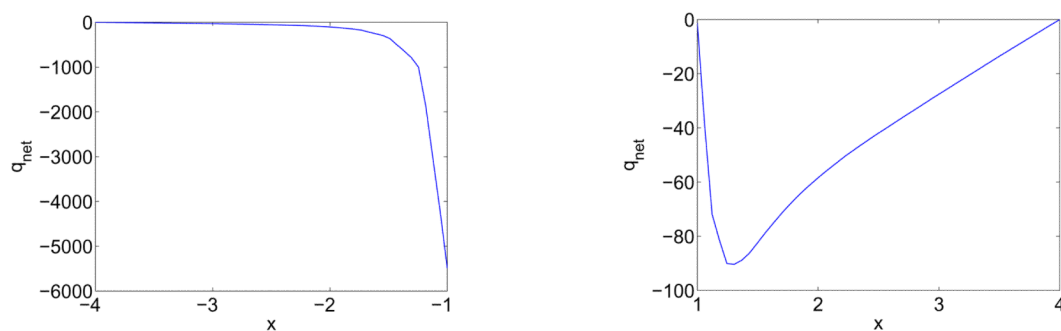
Figure 8.
Left: The surface mesh of the unit sphere on the background of the mesh (pink) of the exterior sphere. The non-reactive boundary is colored cyan and the reactive boundary is colored red. Right: Concentration of the reactive particle on the $x - y$ plane.

Figure 9.
Profiles of the net charge concentration of reactive particles in *mM* along *x*-axis. Left: $-4 \leq x \leq -1$. Right: $1 \leq x \leq 4$.
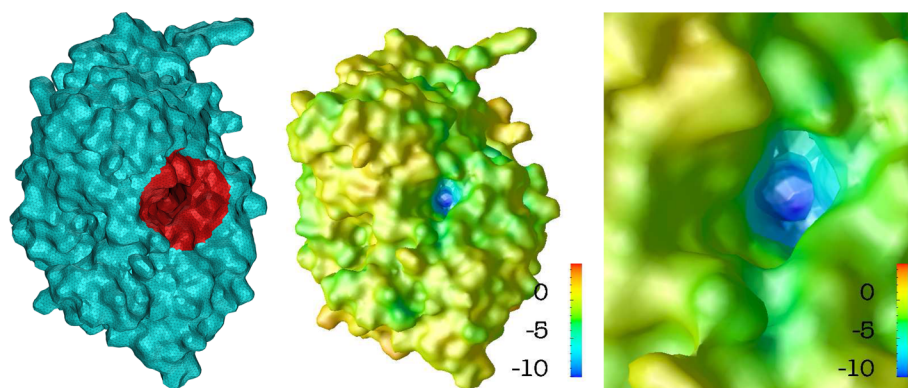
Figure 10.
The discretized molecular surface of AChE with the region around the reaction center colored red (left); The electrostatic potential on the surface (middle) and the surface potential around the reaction center (right).

Table 1

Accuracy of the numerical solutions for Eq. (34).

h_{max}	3.277	1.821	0.965	0.574	0.297
L_2	2.872(−3)	9.747(−4)	2.908(−4)	1.152(−4)	3.271(−4)
Order		1.84	1.90	1.78	1.91
k_r	1.373(11)	1.806(11)	2.149(11)	2.378(11)	2.519(11)

Table 2

L_2 errors between the computed particle concentrations and those predicted by the Boltzmann distribution.

h_{max}	3.277	1.821	0.965	0.574	0.297
$L_2(\rho)$	1.715(−2)	9.437(−3)	5.095(−3)	2.726(−3)	1.280(−3)

Table 3

Numerical error and asymptotic order of convergence for time integration.

Δt	e_φ	order	e_ρ	order
2	5.33(−3)		1.16(−2)	
1	1.47(−3)	1.86	3.65(−3)	1.67
0.5	3.86(−4)	1.93	9.33(−4)	1.97
0.25	1.02(−4)	1.92	2.52(−4)	1.89